Severe immunodeficiency in mice lacking DNA repair factors XLF and Mri

Sergio Castañeda-Zegarra[1,†], Qindong Zhang[1†], Amin Alirezaylavasani[1], Marion Fernandez-Berrocal[1,3], Rouan Yao[1], Valentyn Oksenych[1,2,4,5]*

[1]Department of Clinical and Molecular Medicine (IKOM), Norwegian University of Science and technology, 7491 Trondheim, Norway;

[2]St. Olavs Hospital, Trondheim University Hospital, Clinic of Medicine, Postboks 3250 Sluppen, 7006 Trondheim;

[3]Behavioural Neurobiology MS program, Theodor-Boveri-Institute, Biocenter, University of Würzburg, 97070 Würzburg, Germany.

[4]Department of Biosciences and Nutrition (BioNut), Karolinska Institutet, 14183 Huddinge, Sweden

[5]Institute of Clinical Medicine, UiT The Arctic University of Norway, Tromso, Norway

[†]These authors contributed equally

*Correspondence: valentyn.oksenych@uit.no;

Keywords: NHEJ; Cernunnos; Cyren; pro-B cells; lymphocyte; genetic interaction

Abstract

Non-homologous end joining (NHEJ) is a DNA repair pathway that is required to detect, process, and ligate DNA double-stranded breaks (DSBs) throughout the cell cycle. The NHEJ pathway is necessary for V(D)J recombination in developing B and T lymphocytes. During NHEJ, core factors Ku70 and Ku80 form a heterodimer called Ku, which recognizes DSBs and promotes recruitment and function of downstream factors PAXX, Mri, DNA-PKcs, Artemis, XLF, XRCC4, and Lig4. Mutations in several known NHEJ genes can result in immunodeficient phenotypes, including severe combined immunodeficiency (SCID). Inactivation of *Mri, Paxx* or *Xlf* in mice results in normal or mild phenotype, while combined inactivation of *Xlf/Mri, Xlf/Paxx,* or *Xlf/Dna-pkcs* leads to late embryonic lethality. Here, we demonstrated that deletion of pro-apoptotic factor *Trp53* rescues embryonic lethality in mice with combined deficiency of *Xlf* and *Mri*. Furthermore, *Xlf*$^{-/-}$*Mri*$^{-/-}$*Trp53*$^{+/-}$ mice possessed reduced body weight, severely reduced mature B and T cell counts in the spleen and thymus, and accumulation of progenitor B cells in the bone marrow. Therefore, we conclude that Mri is functionally redundant with XLF during B and T lymphocyte development *in vivo,* and that *Xlf*$^{-/-}$*Mri*$^{-/-}$*Trp53*$^{+/-}$ mice possess a leaky SCID phenotype.

1. Introduction

Non-homologous end-joining (NHEJ) is a DNA repair pathway that recognizes, processes and ligates DNA double-stranded breaks (DSB) throughout the cell cycle. NHEJ is required for lymphocyte development, in particular, to repair DSBs induced by the recombination activating genes (RAG) 1 and 2 in developing B and T lymphocytes, and by activation-induced cytidine deaminase (AID) in mature B cells [1]. NHEJ is initiated when core subunits Ku70 and Ku80 (Ku) are recruited to the DSB sites. Ku, together with DNA-dependent protein kinase, catalytic subunit (DNA-PKcs), form the DNA-PK holoenzyme [2]. Subsequently, the nuclease Artemis is recruited to the DSB sites to process DNA hairpins and overhangs [3]. Finally, DNA ligase IV (Lig4), X-ray repair cross-complementing protein 4 (XRCC4) and XRCC4-like factor (XLF) mediate DNA end ligation. The NHEJ complex is stabilized by a paralogue of XRCC4 and XLF (PAXX) and a modulator of retroviral infection (Mri) [4, 5].

Inactivation of *Ku70*, *Ku80*, *Dna-pkcs* or *Artemis* results in severe combined immunodeficiency (SCID) characterized by lack of mature B and T lymphocytes [2, 3, 6-8]. Deletion of both alleles of *Xrcc4* [9] or *Lig4* [10] results in late embryonic lethality in mice, which correlates with increased apoptosis in the central nervous system (CNS). Inactivation of *Xlf* (*Cernunnos*) results in only a modest immunodeficiency in mice [11-13], while mice lacking *Paxx* [14-17] or *Mri* [5, 18] displayed no overt phenotype.

The mild phenotype observed in mice lacking XLF could be explained by functional redundancy between XLF and multiple DNA repair factors, including *Ataxia telangiectasia* mutated (ATM), histone H2AX [19], Mediator of DNA Damage Checkpoint 1 (MDC1) [20, 21], p53-binding protein 1 (53BP1) [17, 22], RAG2 [23], DNA-PKcs [20, 24, 25], PAXX [4, 14, 15, 20, 26-28] and Mri [5]. However, combined inactivation of *Xlf* and *Paxx* [4, 14, 15, 20], as well as *Xlf* and *Mri* [5], results in late embryonic lethality in mice, presenting a challenge to the study of B and T lymphocyte development *in vivo*. It has also been shown that both embryonic lethality and increased levels of CNS neuronal apoptosis in mice with

deficiency in *Lig4* [9, 10, 29, 30], *Xrcc4* [9, 31], *Xlf* and *Paxx* [20], or *Xlf* and *Dna-pkcs* [24, 25] is p53-dependent.

In this study, we rescue synthetic lethality from *Xlf* and *Mri* by inactivating one or two alleles of *Trp53*. We show that resulting *Xlf*$^{-/-}$*Mri*$^{-/-}$*Trp53*$^{+/-}$ mice possess a leaky SCID phenotype with severely reduced mature B and T lymphocyte counts in the spleen, low mature T cell counts in the thymus, and accumulated progenitor B cells in bone marrow. Finally, we demonstrate that Mri functions in B and T lymphocyte development *in vivo*, and its roles are compensated by XLF.

2. Materials and Methods

2.1. Mice

All experiments involving mice were performed according to the protocols approved by the Comparative Medicine Core Facility (CoMed) at the Norwegian University of Science and Technology (NTNU, Trondheim, Norway). *Xlf*$^{+/-}$ [11] and *Dna-pkcs*$^{+/-}$ [2] mice were imported from the laboratory of Professor Frederick W. Alt at Harvard Medical School. *Trp53*$^{+/-}$ mice [32] were imported from Jackson Laboratories. *Paxx*$^{+/-}$ [16] and *Mri*$^{+/-}$ [18] mice were generated by the Oksenych group and described previously.

2.2. Lymphocyte development

Lymphocyte populations were analyzed by flow cytometry as described previously [16, 18, 19, 22]. In summary, cells were isolated from the spleen, thymus, and femur of 5-7-week-old mice and treated with red blood cell lysis buffer Hybri-Max™ (Sigma Aldrich, St. Louis, MO, USA; #R7757). The cells were resuspended in PBS (Thermo Scientific, Basingstoke, UK; #BR0014G) containing 5% Fetal bovine serum, FCS (Sigma Life Science, St. Louis, Missouri, United States; #F7524), and counted using a Countess™ II Automated Cell Counter (Invitrogen, Carlsbad, CA, United States; #A27977). Then, the cell suspension was diluted with PBS to get a final cell concentration of 2.5 x 10^7 cells per mL. Finally,

surface markers were labeled with fluorochrome-conjugated antibodies and the cell population was analyzed using flow cytometry.

2.3. Class switch recombination

Spleens were isolated from 5-7-week-old mice and stored in cold PBS. Splenocytes were obtained by mincing the spleens; naïve B cells were negatively selected using an EasySep Isolation kit (Stemcell™, Cambridge, UK; #19854). Lipopolysaccharide (LPS; 40 µg/mL; Sigma Aldrich, St. Louis, MO, USA; #437627-5MG) and interleukin 4 (IL-4; 20 ng/mL; PeproTech, Stockholm, Sweden; #214-14) were used to induce CSR to IgG1. Expression of IgG1 was analyzed by flow cytometry.

2.4. Antibodies

The following antibodies were used for flow cytometry analysis: rat anti-CD4-PE-Cy7 (BD Pharmingen™, Allschwil, Switzerland, #552775; 1:100); rat anti-CD8-PE-Cy5 (BD Pharmingen™, Allschwil, Switzerland, #553034; 1:100); anti-CD19-PE-Cy7 (Biolegend, San Diego, CA, USA, #115520; 1:100); hamster anti-mouse anti-CD3-FITC (BD Pharmingen™, Allschwil, Switzerland, #561827; 1:100); rat anti-mouse anti-CD43-FITC (BD Pharmingen™, Allschwil, Switzerland, #561856; 1:100); rat anti-mouse anti-CD45R/B220-APC (BD Pharmingen™, Allschwil, Switzerland; #553092; 1:100); rat anti-mouse anti-IgM-PE-Cy7 (BD Pharmingen™, Allschwil, Switzerland, #552867; 1:100); rat anti-mouse IgG1-APC (BD Pharmingen™, Allschwil, Switzerland; #550874; 1:100). A LIVE/DEAD™ fixable violet dead cell stain kit (ThermoFisher Scientific, Waltham, MA, USA; #L34955; 1:1000) was used to identify dead cells.

2.5. Statistics

Statistical analyses were performed using one-way ANOVA, GraphPad Prism 8.0.1. 244 (San Diego, CA, USA). In all statistical tests, $p<0.05$ were taken to be significant (*$p<0.05$; **$p<0.01$; ***$p<0.001$; ****$p<0.0001$).

3. Results

3.1. Inactivation of Trp53 gene rescued embryonic lethality in mice lacking XLF and Mri

Combined inactivation of *Xlf* and *Mri* has previously been shown to result in synthetic lethality [5]. To generate *Xlf*$^{-/-}$*Mri*$^{-/-}$*Trp53*$^{+/-}$ mice, we intercrossed an *Mri*$^{-/-}$ strain [18] with an *Xlf*$^{-/-}$*Trp53*$^{+/-}$ [20] strain. Next, we selected and intercrossed triple heterozygous (*Xlf*$^{+/-}$*Mri*$^{+/-}$*Trp53*$^{+/-}$), and later, *Xlf*$^{-/-}$*Mri*$^{+/-}$ *Trp53*$^{+/-}$ mice. With PCR screening, we identified among the resulting offsprings *Xlf*$^{-/-}$*Mri*$^{-/-}$*Trp53*$^{+/-}$ (n=6), *Xlf*$^{-/-}$*Mri*$^{-/-}$*Trp53*$^{-/-}$ (n=2), and *Xlf*$^{-/-}$*Mri*$^{-/-}$ (n=1) (Fig. 1). Mice lacking both XLF and Mri possessed reduced weight (12 g on average, $p<0.0001$) when compared with gender- and age-matched WT (19 g), *Xlf*$^{-/-}$ (19 g) and *Mri*$^{-/-}$ (20 g) controls (Fig. 1A,B). We used these XLF/Mri-deficient mice to further characterize the development of B and T lymphocytes *in vivo*.

3.2. Leaky SCID in Xlf$^{-/-}$*Mri*$^{-/-}$*Trp53*$^{+/-}$ *mice*

To determine the roles of Mri in lymphocyte development *in vivo*, we isolated the thymus, spleen, and femur from *Xlf*$^{-/-}$*Mri*$^{-/-}$*Trp53*$^{+/-}$ mice, as well as from the *Xlf*$^{-/-}$, *Mri*$^{-/-}$, *Trp53*$^{+/-}$ and WT controls. Combined deficiency for XLF and Mri resulted in a 3-fold reduction in thymus size (32 mg on average, $p<0.0001$) and 9-fold reduction in thymocyte count (1.9×10^7, $p<0.0001$) when compared to single deficient or WT controls (Fig. 1C). Similarly, both average spleen weight (22 mg, $p<0.0001$) and splenocyte count (2.0×10^7, $p<0.0001$) in *Xlf*$^{-/-}$*Mri*$^{-/-}$*Trp53*$^{+/-}$ mice decreased approximately 4-5 fold when compared with WT and single deficient controls (Fig. 1D). We did not detect any direct influence of *Trp53* genotype on lymphocyte development. The reduced number of splenocytes in XLF/Mri-deficient mice could be explained by decreased populations of B and T lymphocytes observed in the *Xlf*$^{-/-}$*Mri*$^{-/-}$*Trp53*$^{+/-}$ mice (Fig. 1E-G). Specifically, CD3+ T cells were reduced 4-fold ($p<0.0001$), while CD19+ B cells were reduced 20-fold ($p<0.0001$) when compared with single deficient and WT controls (Fig. 1E-G). Likewise, counts of CD4+, CD8+ and CD4+CD8+ T cells in the thymus, as well as counts of CD4+ and CD8+ T cells in the spleen, were all dramatically reduced when compared with single deficient and WT controls (about 4-fold, $p<0.0001$; Fig. 1E,G,H). From these observations, we conclude that XLF and Mri are functionally redundant during B and T lymphocytes development in mice.

3.3. Leaky SCID in mice lacking XLF and PAXX

Combined inactivation of XLF and PAXX has been shown to result in embryonic lethality in mice [4, 14, 15, 20]. To determine the impact of XLF and PAXX on B and T cell development *in vivo*, we rescued the synthetic lethality by inactivating one allele of *Trp53*, as described previously [20]. The resulting *Xlf*$^{-/-}$*Paxx*$^{-/-}$*Trp53*$^{+/-}$ mice possessed 30 to 40-fold reduced thymocyte count (4.0×10^6, $p<0.0001$), when compared to WT (1.3×10^8), *Xlf*$^{-/-}$ (1.4×10^8) and *Paxx*$^{-/-}$ (1.7×10^8) mice. This is reflected in decreased levels of double-positive CD4+CD8+ cells, as well as decreased levels of single-positive CD4+ and CD8+ T cells (Fig. 1,2). Spleen development was dramatically affected in mice lacking XLF and PAXX, compared to WT and single-deficient controls, due to the lack of B cells and decreased T cell count (Fig. 1,2). When compared with the WT and single knockout controls, *Xlf*$^{-/-}$*Paxx*$^{-/-}$*Trp53*$^{+/-}$ mice had a 400- to 600-fold reduction in CD19+ B splenocyte count (0.1×10^6, $p<0.0001$) and a 70- to 90-fold reduction in CD3+ splenocyte count (to 0.3×10^6) (Fig. 1F-H and Fig. 2). From these results, we concluded that XLF and PAXX are functionally redundant during the B and T lymphocyte development in mice.

3.4. Early B cell development is abrogated in mice lacking XLF and Mri, or XLF and PAXX

Reduced counts and proportions of mature B lymphocytes in *Xlf*$^{-/-}$*Mri*$^{-/-}$*Trp53*$^{+/-}$ mice suggest a blockage in B cell development in the bone marrow. To further investigate this, we isolated the bone marrow cells from femora of mice lacking XLF, Mri or both XLF/Mri, and analyzed the proportions of B220+CD43+IgM- progenitor B cells and B220+CD43-IgM+ immature and mature B cells. We detected only background levels of B220+CD43-IgM+ B cells in bone marrows isolated from *Xlf*$^{-/-}$*Mri*$^{-/-}$*Trp53*$^{+/-}$ mice (Fig. 3A,B). However, these mice exhibited a 2- to 3-fold higher proportion of pro-B cells when compared with WT, *Mri*$^{-/-}$ and *Xlf*$^{-/-}$ controls (Fig. 3A,C). Similarly, *Xlf*$^{-/-}$*Paxx*$^{-/-}$*Trp53*$^{+/-}$ mice also possessed background levels of IgM+ B cells ($p<0.0001$; Fig. 3A,B), while having 3- to 4-fold higher proportion of pro-B cells when compared with WT, *Paxx*$^{-/-}$ and *Xlf*$^{-/-}$ controls ($p<0.0001$; Fig. 3A,C).

Therefore, we concluded that B cell development is blocked at the pro-B cell stage of *Xlf*$^{-/-}$*Mri*$^{-/-}$*Trp53*$^{+/-}$ and *Xlf*$^{-/-}$*Paxx*$^{-/-}$*Trp53*$^{+/-}$ mice.

3.5. Normal development of Paxx$^{-/-}$*Mri*$^{-/-}$ *mice*

Both PAXX and Mri are NHEJ factors that are functionally redundant with XLF in mice. Combined inactivation of *Paxx* and *Xlf* [4, 14, 15, 20], or *Mri* and *Xlf* ([5]; this study) results in synthetic lethality in mice, as well as in abrogated V(D)J recombination in vAbl pre-B cells [4, 5, 14, 15, 27]. To determine if *Paxx* genetically interacts with *Mri*, we intercrossed mice that are heterozygous or null for both genes (e.g., *Paxx*$^{+/-}$*Mri*$^{+/-}$). We found that resulting *Paxx*$^{-/-}$*Mri*$^{-/-}$ mice are live-born, fertile, and similar to WT littermates by size (17 g, $p>0.9999$) (Fig. 4A,B). *Paxx*$^{-/-}$*Mri*$^{-/-}$ mice underwent normal B and T cell development, indistinguishable from the WT, *Paxx*$^{-/-}$, and *Mri*$^{-/-}$ controls (Fig. 1F-H and 4C). Specifically, we observed that *Paxx*$^{-/-}$*Mri*$^{-/-}$ mice had normal thymocyte and splenocyte counts, which encompass CD4+, CD8+, and CD4+CD8+ T cells and CD19+ B cells (Fig. 4C). *Paxx* inactivation did not affect Ig switch to IgG1 in *Mri*-deficient B cells (Fig. 4D,E). The quantity of IgG1+ cells after CSR stimulation was similar between *Paxx*$^{-/-}$*Mri*$^{-/-}$ and *Mri*$^{-/-}$ naïve B cells ($p>0.48$), although both were lower than that of WT control, at 72 h and 96 h ($p<0.05$). From this, we can conclude that there is no genetic interaction between *Paxx* and *Mri in vivo*.

3.6. Synthetic lethality between Mri and Dna-pkcs in mice

Both Mri and DNA-PKcs are functionally redundant with XLF in mouse development [5, 24]. Combined inactivation of *Paxx* and *Mri* (this study), or *Paxx* and *Dna-pkcs* [20] genes results in live-born mice that are indistinguishable from single deficient controls. To determine if *Mri* genetically interacts with *Dna-pkcs*, we crossed *Mri*$^{+/-}$ and *Dna-pkcs*$^{+/-}$ mouse strains, then intercrossed the double-heterozygous and *Mri*$^{-/-}$*Dna-pkcs*$^{+/-}$ strains (Fig. 5A). We identified 12 *Mri*$^{-/-}$*Dna-pkcs*$^{+/+}$ mice and 12 *Mri*$^{-/-}$*Dna-pkcs*$^{+/-}$ mice, but no *Mri*$^{-/-}$*Dna-pkcs*$^{-/-}$ mice (out of 6 expected). To determine if double-deficient *Mri*$^{-/-}$*Dna-pkcs*$^{-/-}$ embryos are present at day E14.5, we intercrossed *Mri*$^{-/-}$*Dna-pkcs*$^{+/-}$ mice and analyzed embryos (Fig. 5B). We identified two *Mri*$^{-/-}$*Dna-pkcs*$^{-/-}$ embryos (63mg), which were

about 40% lighter than *Mri*$^{-/-}$ embryos (108mg) (Fig. 5C,D). A Chi-Square test ($\chi 2$) was performed to determine if the embryonic distribution data fits the mendelian ratio of 1:2:1 that is expected from *Mri*$^{-/-}$*Dna-pkcs*$^{+/-}$ parents. With DF=2 and $\chi 2$=1.8, the corresponding p-value lies within the range $0.25<p<0.5$. This affirms that our data fit the expected 1:2:1 distribution and suggests that *Mri*$^{-/-}$*Dna-pkcs*$^{-/-}$ is synthetic lethal. Therefore, we can conclude that there is genetic interaction between *Mri* and *Dna-pkcs in vivo*.

4. Discussion

Genetic inactivation of *Xlf* [11], *Paxx* [4, 14-16], or *Mri* [5, 33] in mice leads to development of modest or no detectable phenotype. However, inactivation of other NHEJ factors, such as *Ku70*$^{-/-}$ [6], *Ku80*$^{-/-}$ [7], *Artemis*$^{-/-}$ [3], *Dna-pkcs*$^{-/-}$ [2] results in blockage of B and T cell development in mice, while inactivation of *Xrcc4* [9] and *Lig4* [10] results in embryonic lethality. Moreover, combined inactivation of *Xlf* and *Mri* [5], *Xlf* and *Paxx* [4, 14, 15], or *Xlf* and *Dna-pkcs* [24, 25] also results in embryonic lethality, which is correlated with increased levels of neuronal apoptosis in the central nervous system (Fig. 6). In addition, *Xlf* genetically interacts with RAG2 [23] and DDR factors, such as *Atm*, *53bp1*, *H2ax,* and *Mdc1* [17, 19-22, 34]. *Xlf*$^{-/-}$*Rag2*$^{-/-}$ mice almost completely lack mature B cells and have significantly fewer mature T cells than single deficient controls [23]. *Xlf*$^{-/-}$*Atm*$^{-/-}$ and *Xlf*$^{-/-}$*53bp1*$^{-/-}$ mice are live-born and exhibit reduced body weight, increased genomic instability, and severe lymphocytopenia as a result of V(D)J recombination impairment in developing B and T cells [1, 17, 19, 22]. In contrast, *Xlf*$^{-/-}$*H2ax*$^{-/-}$ and *Xlf*$^{-/-}$*Mdc1*$^{-/-}$ mice are embryonic lethal [19-21]. There are several possible explanations for the functional redundancy observed between DNA repair genes. For instance, the two factors could have identical (e.g., if both proteins are involved in ligation or DNA end tethering) or complementary (e.g. if one protein stimulates ligation while the other is required for DNA end tethering) functions. To date, XLF has been shown to genetically interact with multiple DNA repair factors [1, 4, 5, 14, 15, 19, 20, 24, 25, 35], and this list is likely to grow [34, 36]. However, no clear genetic interaction has been shown between *Xlf* and *Artemis* or *Xrcc4* in the context of mouse development and V(D)J

recombination [24], meaning that it remains difficult to predict genetic interactions without developing and characterizing genetic models.

Inactivation of one or two alleles of *Trp53* rescues the embryonic lethality of *Xrcc4*$^{-/-}$[9, 31], *Lig4*$^{-/-}$[10, 30], *Xlf*$^{-/-}$*Dna-pkcs*$^{-/-}$ and *Xlf*$^{-/-}$*Paxx*$^{-/-}$[20] (Fig. 6). Recent findings suggest that Mri forms heterogeneous complexes containing PAXX or XLF, which function during DNA DSB repair by the NHEJ [5]. Additionally, combined inactivation of *Xlf* and *Mri* in vAbl pre-B cells results in a severe block in V(D)J recombination and accumulation of unrepaired DNA double-strand breaks *in vitro,* although whether combined inactivation of *Xlf* and *Mri* could result in the lack of B and t lymphocytes in adult mice remained unclear [5]. Similarly, double deficient vAbl pre-B cells lacking *Xlf* and *Paxx* are unable to sustain V(D)J recombination. Importantly, the lack of a progenitor T cell model system left the question of T cell development in *Xlf*$^{-/-}$*Mri*$^{-/-}$ and *Xlf*$^{-/-}$*Paxx*$^{-/-}$ mice completely unexplored. Inactivation of *Trp53* resulted in live-born mice lacking XLF/PAXX [20]. These *Xlf*$^{-/-}$*Paxx*$^{-/-}$*Trp53*$^{-/-}$ mice had nearly no B and T cells, reduced size of spleen and hardly detectable thymus [20] (Fig. 6). Moreover, a conditional knockout mouse model, which results in double-deficiency of XLF/PAXX in early hematopoietic progenitor cells only, was also able to overcome the embryonic lethality of *Xlf*$^{-/-}$*Paxx*$^{-/-}$ mice [37]. With this model, impairment of V(D)J recombination in *Xlf*$^{-/-}$*Paxx*$^{-/-}$ cells, as well as the resulting depletion of mature B cells and lack of a visible thymus could also be observed *in vivo* [37].

We have demonstrated that mice lacking XLF, Mri and p53, although live-born, possess a leaky SCID phenotype. *Xlf*$^{-/-}$*Mri*$^{-/-}$*Trp53*$^{+/-}$ mice have a clear fraction of mature B cells in the spleens (CD19+) and bone marrow (B220+CD43-IgM+) (Fig. 1,3,6), as well as clear fractions of double and single-positive T cells in the thymus (CD4+CD8+, CD4+, CD8+) and single-positive T cells in the spleen (CD4+ and CD8+) (Fig. 1). However, the cell fractions from these mice are noticeably smaller than those of WT or single-deficient mice. Similarly, *Xlf*$^{-/-}$*Paxx*$^{-/-}$*Trp53*$^{+/-}$ mice are also live-born and possess a very small number of mature B cells in the spleen and bone marrow, as well as very minor fractions of single positive T cells in thymus and spleen (Fig. 2,3,6). Due to the smaller presence of mature B and T

cells in these mice, we categorize the observed immunodeficient phenotypes as “leaky SCID”, which has previously been described in mice lacking other NHEJ factors, such as *Ku70*$^{-/-}$ [6], *Artemis*$^{-/-}$ [3], *Lig4*$^{-/-}$*Trp53*$^{-/-}$, *Xrcc4*$^{-/-}$*Trp53*$^{-/-}$ [9, 31], *Xlf*$^{-/-}$*Atm*$^{-/-}$ [19] *and Xlf*$^{-/-}$*Rag2*$^{-/-}$ [23]. It is important to note that inactivation of *Trp53* is not always sufficient to rescue embryonic lethality in mice; for example, PLK1-interacting checkpoint helicase (PICH)-deficient mice possess developmental defects in the presence or absence of p53 [38]. Moreover, ATR mutants (Seckel syndrome) are not completely rescued from embryonic lethality with the inactivation of *Trp53* [39].

We also found that mice with combined inactivation of *Paxx* and *Mri* (*Paxx*$^{-/-}$*Mri*$^{-/-}$) are live-born, fertile, and undergo nearly normal B and T cell development (Fig. 4). Moreover, inactivation of *Paxx* did not affect the CSR efficiency in *in vitro* stimulated Mri-deficient B cells (Fig. 4), thereby confirming our observations *in vitro*. It has been shown that combined inactivation of *Paxx* and *Mri* genes in vAbl pre-B cells lead to similar V(D)J recombination efficiency to single deficient *Mri*$^{-/-}$, *Paxx*$^{-/-}$ and WT controls [5]. Furthermore, combined inactivation of *Paxx* and *Ku80* (*Paxx*$^{-/-}$*Ku80*$^{-/-}$), or *Paxx Atm* (*Paxx*$^{-/-}$*Atm*$^{-/-}$) [15], as well as *Paxx* and *Dna-pkcs* (*Paxx*$^{-/-}$*Dna-pkcs*$^{-/-}$) [20] lead to a phenotype similar to their single deficient controls, *Ku80*$^{-/-}$, *Atm*$^{-/-}$ and *Dna-pkcs*$^{-/-}$, correspondingly. Thus, while *Paxx* and *Mri* both interact genetically with *Xlf*, we conclude that they do not interact with each other.

Both *Mri* an *Dna-pkcs* genetically interact with *Xlf*. Strikingly, we found that combined inactivation of *Mri* and *Dna-pkcs* (*Mri*$^{-/-}$*Dna-pkcs*$^{-/-}$) leads to embryonic lethality, and that E14.5 *Mri*$^{-/-}$*Dna-pkcs*$^{-/-}$ murine embryos were about 40% smaller than single-deficient siblings. DNA-PKcs is associated with the N-terminus of the Mri and Ku heterodimer in the process of recognizing DSBs [5], which may account for genetic interaction between *Mri* and *Dna-pkcs*. Thus, inactivation of *Trp53, Ku70* or *Ku80* may be a viable method to rescue synthetic lethality from *Mri*$^{-/-}$*Dna-pkcs*$^{-/-}$ mice.

Xlf and *Mri* interact genetically, and mice lacking XLF/Mri are embryonic lethal, which was demonstrated by *Hung et al. (2018)* [5] and in current study. Nevertheless, we identified one *Xlf*$^{-/-}$*Mri*$^{-/-}$*Trp53*$^{+/+}$ mouse at age of 30 days. This mouse resembled *Xlf*$^{-/-}$*Mri*$^{-/-}$*Trp53*$^{+/-}$ and *Xlf*$^{-/-}$*Mri*$^{-/-}$*Trp53*$^{-/-}$ mice

of similar age with respect of B and T cell development; however, it was sicker in general and had to be euthanized (Fig. 1, 6). Similarly, one live-born *Xlf*$^{-/-}$*Paxx*$^{-/-}$ mouse was reported by *Balmus et al. (2016)* [15],indicating that, exceptionally, embryonic lethality in NHEJ-deficient mice can be overcome, likely due to activity of alternative end-joining.

In conclusion, we have developed several complex genetic models (Fig. 6). *Xlf*$^{-/-}$*Mri*$^{-/-}$*Trp53*$^{+/-}$ and *Xlf*$^{-/-}$*Paxx*$^{-/-}$*Trp53*$^{+/-}$ mice possessed severely impaired B and T lymphocyte development; *Mri*$^{-/-}$*Paxx*$^{-/-}$ mice develop phenotypes similar to single-deficient controls; and *Mri*$^{-/-}$*Dna-pkcs*$^{-/-}$ mice are embryonic lethal.

Author contributions

VO, SCZ, QZ, AL and MFB designed the study, analyzed and interpreted the results. SCZ, QZ, AL and MFB performed most of the experiments. VO wrote the paper with the help of SCZ, QZ and RY. All the authors contributed to writing of the final manuscript.

Conflict of interest statement

The authors declare no conflict of interest.

Acknowledgments

This work was supported by the Research Council of Norway Young Talent Investigator grant (#249774) to V.O. In addition, VO group was supported by the Liaison Committee for Education, Research, and Innovation in Central Norway (#13477; #38811); the Norwegian Cancer Society (#182355); the Research Council of Norway FRIMEDBIO grants (#270491 and #291217), and The Outstanding Academic Fellow Program at NTNU (2017–2021).

Figure legends

Fig. 1. B and T cell development in *Xlf*$^{-/-}$*Mri*$^{-/-}$*Trp53*$^{+/-}$ mice. (A) Comparison of body size, thymi and spleens of XLF/Mri-deficient and XLF-deficient mice of the same age. (B) Weights of WT, *Xlf*$^{-/-}$, *Mri*$^{-/-}$,

Xlf$^{-/-}$*Mri*$^{-/-}$*Trp53*$^{+/-}$ mice. (C, D) Number (×10^6) of thymocytes (C) and splenocytes (D) in WT, *Xlf*$^{-/-}$, *Mri*$^{-/-}$, *Xlf*$^{-/-}$*Mri*$^{-/-}$*Trp53*$^{+/-}$ mice. (E) Flow cytometric analysis of thymic and splenic T cell subsets and splenic CD19+ B cells. (F,G,H) Number (×10^6) of splenic CD19+ B cells (F), splenic CD3+ T cells (G) and thymic CD4+CD8+ double positive (DP) T cells (H) in WT, *Xlf*$^{-/-}$, *Mri*$^{-/-}$, *Xlf*$^{-/-}$*Mri*$^{-/-}$*Trp53*$^{+/-}$ mice. Comparisons between every two groups were made using one-way ANOVA, GraphPad Prism 8.0.1. *Xlf*$^{-/-}$*Mri*$^{-/-}$*Trp53*$^{-}$ is a combination of *Xlf*$^{-/-}$*Mri*$^{-/-}$*Trp53*$^{+/-}$ and *Xlf*$^{-/-}$*Mri*$^{-/-}$*Trp53*$^{-/-}$. *Xlf*$^{-/-}$*Paxx*$^{-/-}$*Trp53*$^{-}$ is a combination of *Xlf*$^{-/-}$*Paxx*$^{-/-}$*Trp53*$^{+/-}$ and *Xlf*$^{-/-}$*Paxx*$^{-/-}$*Trp53*$^{-/-}$.

Fig. 2. B and T cell development in *Xlf*$^{-/-}$*Paxx*$^{-/-}$*Trp53*$^{+/-}$ mice. Examples of flow cytometric analysis of thymic and splenic T cell subsets and splenic CD19+ B cells.

Fig. 3. B cell development is abrogated in bone marrow of *Xlf*$^{-/-}$*Mri*$^{-/-}$*Trp53*$^{+/-}$ and *Xlf*$^{-/-}$*Paxx*$^{-/-}$*Trp53*$^{+/-}$ mice. (A) Flow cytometric analysis of developing B cells. Upper left box marks progenitor B cell population and lower right box marks the IgM+ B cells. (B, C) Frequencies (%) of IgM+ B cells (B) and progenitor B cells (C) in WT, *Xlf*$^{-/-}$, *Mri*$^{-/-}$, *Xlf*$^{-/-}$*Mri*$^{-/-}$*Trp53*$^{+/-}$, *Paxx*$^{-/-}$, and *Xlf*$^{-/-}$*Paxx*$^{-/-}$*Trp53*$^{+/-}$ mice. Comparisons between groups were made using one-way ANOVA, GraphPad Prism 8.0.1. *Xlf*$^{-/-}$*Mri*$^{-/-}$*Trp53*$^{-}$ is a combination of *Xlf*$^{-/-}$*Mri*$^{-/-}$*Trp53*$^{+/-}$ and *Xlf*$^{-/-}$*Mri*$^{-/-}$*Trp53*$^{-/-}$. *Xlf*$^{-/-}$*Paxx*$^{-/-}$*Trp53*$^{-}$ is a combination of *Xlf*$^{-/-}$*Paxx*$^{-/-}$*Trp53*$^{+/-}$ and *Xlf*$^{-/-}$*Paxx*$^{-/-}$*Trp53*$^{-/-}$.

Fig. 4. B and T cell development in *Paxx*$^{-/-}$*Mri*$^{-/-}$ mice. (A) Number of thirty-day-old mice (P30) of indicated genotypes. Parents were *Paxx*$^{+/-}$*Mri*$^{+/-}$ and *Paxx*$^{-/-}$*Mri*$^{+/-}$. (B) Example of thirty-day-old *Mri*$^{-/-}$*Paxx*$^{-/-}$ and WT male littermates with their respective thymi and spleens. (C) Example of flow cytometry analyzes of B and T cells in *Paxx*$^{-/-}$*Mri*$^{-/-}$ and WT mice. (D,E) Class switching analyzes of *in vitro* activated naïve B cells of indicated genotypes.

Fig. 5. Genetic interaction between *Mri* and *Dna-pkcs in vivo*. (A) No live-born *Mri*$^{-/-}$*Dna-pkcs*$^{-/-}$ mice were detected. (B,C) *Mri*$^{-/-}$*Dna-pkcs*$^{-/-}$ embryos were detected at day E14.5. (D) Body weight in milligrams (mg) from two E14.5 *Mri*$^{-/-}$*Dna-pkcs*$^{-/-}$ and *Mri*$^{-/-}$*Dna-pkc*$^{+/-}$ embryos from the same litter. The

mendelian ratio 1:2:1 in embryos was verified by the Chi-Square test ($\chi 2$). The $\chi 2$ was 1.8 and its corresponding probability was between 25 and 50%. *Expected distribution assuming lethality.

Fig. 6. Mutations in NHEJ genes result in different phenotypes. Suggested models. Inactivation of *Paxx* or *Mri* results in live-born mice with nearly no DNA repair defects. Inactivation of *Xlf* or *Dna-pkcs* results in live-born mice with increased levels of genomic instability due to reduced NHEJ activity. Combined inactivation of *Xlf/Paxx*, *Xlf/Mri* and *Xlf/Dna-pkcs* leads to embryonic lethality in mice that correlate with high levels of genomic instability and nearly no NHEJ. Accumulated DSBs activate the DNA damage response (DDR) pathway that triggers cell cycle arrest and apoptosis. Alternative end-joining is blocked by presence of Ku70/Ku80. Inactivation of one or two alleles of *Trp53* rescues embryonic lethality of *Xlf/Paxx*, *Xlf/Mri* and *Xlf/Dna-pkcs* mice. This embryonic lethality is likely to be rescued by inactivation of *Ku70* or *Ku80*.

References

1. Kumar V, Alt FW, Oksenych V. Functional overlaps between XLF and the ATM-dependent DNA double strand break response. DNA Repair (Amst). 2014; 16: 11-22. https://doi.org:10.1016/j.dnarep.2014.01.010
2. Gao Y, Chaudhuri J, Zhu C, Davidson L, Weaver DT, Alt FW. A targeted DNA-PKcs-null mutation reveals DNA-PK-independent functions for KU in V(D)J recombination. Immunity. 1998; 9: 367-76. https://doi.org:10.1016/s1074-7613(00)80619-6
3. Rooney S, Sekiguchi J, Zhu C, Cheng HL, Manis J, Whitlow S, DeVido J, Foy D, Chaudhuri J, Lombard D, Alt FW. Leaky Scid phenotype associated with defective V(D)J coding end processing in Artemis-deficient mice. Mol Cell. 2002; 10: 1379-90. https://doi.org:10.1016/s1097-2765(02)00755-4
4. Liu X, Shao Z, Jiang W, Lee BJ, Zha S. PAXX promotes KU accumulation at DNA breaks and is essential for end-joining in XLF-deficient mice. Nat Commun. 2017; 8: 13816. https://doi.org:10.1038/ncomms13816
5. Hung PJ, Johnson B, Chen BR, Byrum AK, Bredemeyer AL, Yewdell WT, Johnson TE, Lee BJ, Deivasigamani S, Hindi I, Amatya P, Gross ML, Paull TT, et al. MRI Is a DNA Damage Response Adaptor during Classical Non-homologous End Joining. Mol Cell. 2018; 71: 332-42 e8. https://doi.org:10.1016/j.molcel.2018.06.018
6. Gu Y, Seidl KJ, Rathbun GA, Zhu C, Manis JP, van der Stoep N, Davidson L, Cheng HL, Sekiguchi JM, Frank K, Stanhope-Baker P, Schlissel MS, Roth DB, et al. Growth retardation and leaky SCID phenotype of Ku70-deficient mice. Immunity. 1997; 7: 653-65. https://doi.org:10.1016/S1074-7613(00)80386-6
7. Nussenzweig A, Chen C, da Costa Soares V, Sanchez M, Sokol K, Nussenzweig MC, Li GC. Requirement for Ku80 in growth and immunoglobulin V(D)J recombination. Nature. 1996; 382: 551-5. https://doi.org:10.1038/382551a0
8. Ma Y, Pannicke U, Schwarz K, Lieber MR. Hairpin opening and overhang processing by an Artemis/DNA-dependent protein kinase complex in nonhomologous end joining and V(D)J recombination. Cell. 2002; 108: 781-94. https://doi.org:10.1016/s0092-8674(02)00671-2

9. Gao Y, Sun Y, Frank KM, Dikkes P, Fujiwara Y, Seidl KJ, Sekiguchi JM, Rathbun GA, Swat W, Wang J, Bronson RT, Malynn BA, Bryans M, et al. A critical role for DNA end-joining proteins in both lymphogenesis and neurogenesis. Cell. 1998; 95: 891-902. https://doi.org:10.1016/s0092-8674(00)81714-6
10. Frank KM, Sekiguchi JM, Seidl KJ, Swat W, Rathbun GA, Cheng HL, Davidson L, Kangaloo L, Alt FW. Late embryonic lethality and impaired V(D)J recombination in mice lacking DNA ligase IV. Nature. 1998; 396: 173-7. https://doi.org:10.1038/24172
11. Li G, Alt FW, Cheng HL, Brush JW, Goff PH, Murphy MM, Franco S, Zhang Y, Zha S. Lymphocyte-specific compensation for XLF/cernunnos end-joining functions in V(D)J recombination. Mol Cell. 2008; 31: 631-40. https://doi.org:10.1016/j.molcel.2008.07.017
12. Vera G, Rivera-Munoz P, Abramowski V, Malivert L, Lim A, Bole-Feysot C, Martin C, Florkin B, Latour S, Revy P, de Villartay JP. Cernunnos deficiency reduces thymocyte life span and alters the T cell repertoire in mice and humans. Mol Cell Biol. 2013; 33: 701-11. https://doi.org:10.1128/MCB.01057-12
13. Roch B, Abramowski V, Chaumeil J, de Villartay JP. Cernunnos/Xlf Deficiency Results in Suboptimal V(D)J Recombination and Impaired Lymphoid Development in Mice. Front Immunol. 2019; 10: 443. https://doi.org:10.3389/fimmu.2019.00443
14. Abramowski V, Etienne O, Elsaid R, Yang J, Berland A, Kermasson L, Roch B, Musilli S, Moussu JP, Lipson-Ruffert K, Revy P, Cumano A, Boussin FD, et al. PAXX and Xlf interplay revealed by impaired CNS development and immunodeficiency of double KO mice. Cell Death Differ. 2018; 25: 444-52. https://doi.org:10.1038/cdd.2017.184
15. Balmus G, Barros AC, Wijnhoven PW, Lescale C, Hasse HL, Boroviak K, le Sage C, Doe B, Speak AO, Galli A, Jacobsen M, Deriano L, Adams DJ, et al. Synthetic lethality between PAXX and XLF in mammalian development. Genes Dev. 2016; 30: 2152-7. https://doi.org:10.1101/gad.290510.116
16. Gago-Fuentes R, Xing M, Saeterstad S, Sarno A, Dewan A, Beck C, Bradamante S, Bjoras M, Oksenych V. Normal development of mice lacking PAXX, the paralogue of XRCC4 and XLF. FEBS Open Bio. 2018; 8: 426-34. https://doi.org:10.1002/2211-5463.12381
17. Liu X, Jiang W, Dubois RL, Yamamoto K, Wolner Z, Zha S. Overlapping functions between XLF repair protein and 53BP1 DNA damage response factor in end joining and lymphocyte development. Proc Natl Acad Sci U S A. 2012; 109: 3903-8. https://doi.org:10.1073/pnas.1120160109
18. Castaneda-Zegarra S, Huse C, Rosand O, Sarno A, Xing M, Gago-Fuentes R, Zhang Q, Alirezaylavasani A, Werner J, Ji P, Liabakk NB, Wang W, Bjoras M, et al. Generation of a Mouse Model Lacking the Non-Homologous End-Joining Factor Mri/Cyren. Biomolecules. 2019; 9. https://doi.org:10.3390/biom9120798
19. Zha S, Guo C, Boboila C, Oksenych V, Cheng HL, Zhang Y, Wesemann DR, Yuen G, Patel H, Goff PH, Dubois RL, Alt FW. ATM damage response and XLF repair factor are functionally redundant in joining DNA breaks. Nature. 2011; 469: 250-4. https://doi.org:10.1038/nature09604
20. Castaneda-Zegarra S, Xing M, Gago-Fuentes R, Saeterstad S, Oksenych V. Synthetic lethality between DNA repair factors Xlf and Paxx is rescued by inactivation of Trp53. DNA Repair (Amst). 2019; 73: 164-9. https://doi.org:10.1016/j.dnarep.2018.12.002
21. Beck C, Castaneda-Zegarra S, Huse C, Xing M, Oksenych V. Mediator of DNA Damage Checkpoint Protein 1 Facilitates V(D)J Recombination in Cells Lacking DNA Repair Factor XLF. Biomolecules. 2019; 10. https://doi.org:10.3390/biom10010060
22. Oksenych V, Alt FW, Kumar V, Schwer B, Wesemann DR, Hansen E, Patel H, Su A, Guo C. Functional redundancy between repair factor XLF and damage response mediator 53BP1 in V(D)J recombination and DNA repair. Proc Natl Acad Sci U S A. 2012; 109: 2455-60. https://doi.org:10.1073/pnas.1121458109
23. Lescale C, Abramowski V, Bedora-Faure M, Murigneux V, Vera G, Roth DB, Revy P, de Villartay JP, Deriano L. RAG2 and XLF/Cernunnos interplay reveals a novel role for the RAG complex in DNA repair. Nat Commun. 2016; 7: 10529. https://doi.org:10.1038/ncomms10529

24. Oksenych V, Kumar V, Liu X, Guo C, Schwer B, Zha S, Alt FW. Functional redundancy between the XLF and DNA-PKcs DNA repair factors in V(D)J recombination and nonhomologous DNA end joining. Proc Natl Acad Sci U S A. 2013; 110: 2234-9. https://doi.org:10.1073/pnas.1222573110
25. Xing M, Bjoras M, Daniel JA, Alt FW, Oksenych V. Synthetic lethality between murine DNA repair factors XLF and DNA-PKcs is rescued by inactivation of Ku70. DNA Repair (Amst). 2017; 57: 133-8. https://doi.org:10.1016/j.dnarep.2017.07.008
26. Lescale C, Lenden Hasse H, Blackford AN, Balmus G, Bianchi JJ, Yu W, Bacoccina L, Jarade A, Clouin C, Sivapalan R, Reina-San-Martin B, Jackson SP, Deriano L. Specific Roles of XRCC4 Paralogs PAXX and XLF during V(D)J Recombination. Cell Rep. 2016; 16: 2967-79. https://doi.org:10.1016/j.celrep.2016.08.069
27. Kumar V, Alt FW, Frock RL. PAXX and XLF DNA repair factors are functionally redundant in joining DNA breaks in a G1-arrested progenitor B-cell line. Proc Natl Acad Sci U S A. 2016; 113: 10619-24. https://doi.org:10.1073/pnas.1611882113
28. Hung PJ, Chen BR, George R, Liberman C, Morales AJ, Colon-Ortiz P, Tyler JK, Sleckman BP, Bredemeyer AL. Deficiency of XLF and PAXX prevents DNA double-strand break repair by non-homologous end joining in lymphocytes. Cell Cycle. 2017; 16: 286-95. https://doi.org:10.1080/15384101.2016.1253640
29. Barnes DE, Stamp G, Rosewell I, Denzel A, Lindahl T. Targeted disruption of the gene encoding DNA ligase IV leads to lethality in embryonic mice. Curr Biol. 1998; 8: 1395-8. https://doi.org:10.1016/s0960-9822(98)00021-9
30. Frank KM, Sharpless NE, Gao Y, Sekiguchi JM, Ferguson DO, Zhu C, Manis JP, Horner J, DePinho RA, Alt FW. DNA ligase IV deficiency in mice leads to defective neurogenesis and embryonic lethality via the p53 pathway. Mol Cell. 2000; 5: 993-1002. https://doi.org:10.1016/s1097-2765(00)80264-6
31. Gao Y, Ferguson DO, Xie W, Manis JP, Sekiguchi J, Frank KM, Chaudhuri J, Horner J, DePinho RA, Alt FW. Interplay of p53 and DNA-repair protein XRCC4 in tumorigenesis, genomic stability and development. Nature. 2000; 404: 897-900. https://doi.org:10.1038/35009138
32. Jacks T, Remington L, Williams BO, Schmitt EM, Halachmi S, Bronson RT, Weinberg RA. Tumor spectrum analysis in p53-mutant mice. Curr Biol. 1994; 4: 1-7. https://doi.org:10.1016/s0960-9822(00)00002-6
33. Castaneda-Zegarra S, Huse C, Røsand Ø, Sarno A, Xing M, Gago-Fuentes R, Zhang Q, Alirezaylavasani A, Werner J, Ji P, Liabakk N, Wang W, Bjørås M, et al. Generation of a Mouse Model Lacking the Non-Homologous End-Joining Factor Mri/Cyren. *Biomolecules*. 2019; 9. https://doi.org:10.3390/biom9120798
34. Castañeda-Zegarra S, Fernandez-Berrocal M, Tkachov M, Yao R, Esnardo Upfold NL, Oksenych V. Genetic Interaction Between the Non-homologous End Joining Factors during B and T Lymphocyte Development: In Vivo Mouse Models. Preprints. 2020. https://doi.org:10.20944/preprints202005.0277.v1
35. Castañeda-Zegarra S, Zhang Q, Alirezaylavasani A, Oksenych V. Leaky severe combined immunodeficiency in mice lacking non-homologous end joining factors XLF and Mri. bioRxiv. 2020: 2020.03.04.976829. https://doi.org:10.1101/2020.03.04.976829
36. Wang X, Lee B, Zha S. The recent advances in non-homologous end-joining through the lens of lymphocyte development. DNA Repair (Amst). 2020. https://doi.org:10.1016/j.dnarep.2020.102874
37. Musilli S, Abramowski V, Roch B, de Villartay JP. An in vivo study of the impact of deficiency in the DNA repair proteins PAXX and XLF on development and maturation of the hemolymphoid system. J Biol Chem. 2020; 295: 2398-406. https://doi.org:10.1074/jbc.AC119.010924
38. Albers E, Sbroggio M, Pladevall-Morera D, Bizard AH, Avram A, Gonzalez P, Martin-Gonzalez J, Hickson ID, Lopez-Contreras AJ. Loss of PICH Results in Chromosomal Instability, p53 Activation, and Embryonic Lethality. Cell Rep. 2018; 24: 3274-84. https://doi.org:10.1016/j.celrep.2018.08.071

39. Murga M, Bunting S, Montana MF, Soria R, Mulero F, Canamero M, Lee Y, McKinnon PJ, Nussenzweig A, Fernandez-Capetillo O. A mouse model of ATR-Seckel shows embryonic replicative stress and accelerated aging. Nat Genet. 2009; 41: 891-8. https://doi.org:10.1038/ng.420

Figure 1

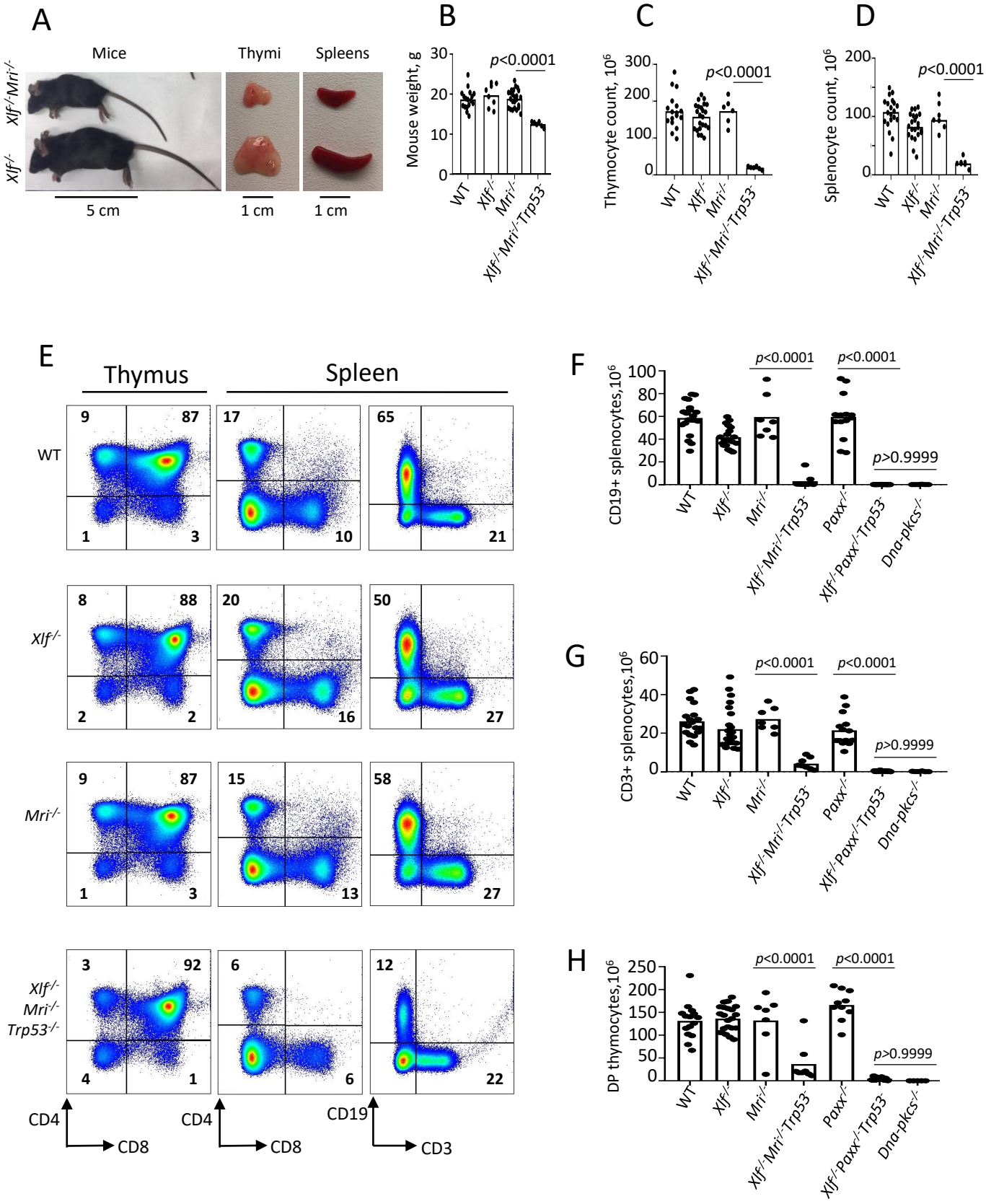
A
Mice
Thymi
Spleens
Xlf-/-Mri-/-
Xlf-/-
5 cm
1 cm
1 cm
B
Mouse weight, g
p<0.0001
WT
Xlf-/-
Mri-/-
Xlf-/-Mri-/-Trp53-
C
Thymocyte count, 10^6
p<0.0001
D
Splenocyte count, 10^6
p<0.0001
E
Thymus
Spleen
WT
Xlf-/-
Mri-/-
Xlf-/-
Mri-/-
Trp53-/-
CD4
CD8
CD19
CD3
F
CD19+ splenocytes,10^6
p<0.0001
p<0.0001
p>0.9999
Paxx-/-
Dna-pkcs-/-
Xlf-/-Paxx-/-Trp53-
G
CD3+ splenocytes,10^6
H
DP thymocytes,10^6

Figure 2

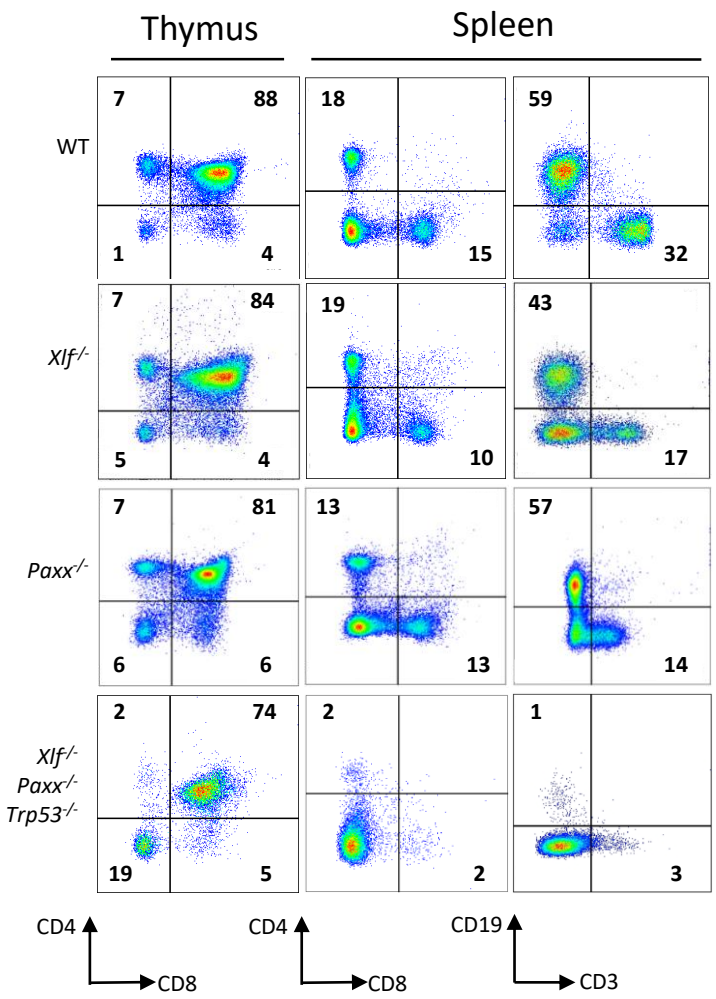
Thymus
Spleen
WT
Xlf-/-
Paxx-/-
Xlf-/-
Paxx-/-
Trp53-/-
7
88
1
4
18
15
59
32
7
84
5
4
19
10
43
17
7
81
6
6
13
13
57
14
2
74
19
5
2
2
1
3
CD4
CD8
CD4
CD8
CD19
CD3

Figure 3

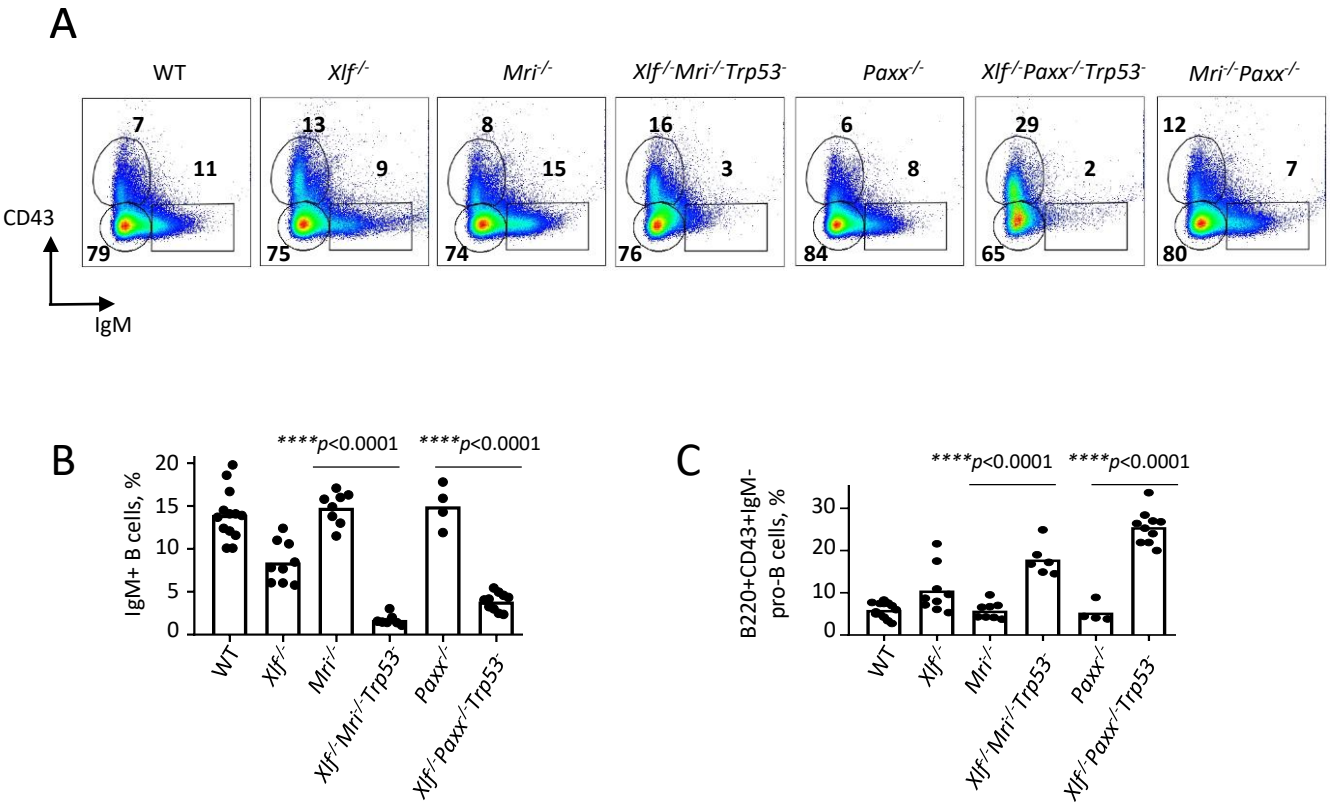
A
WT
Xlf-/-
Mri-/-
Xlf-/-Mri-/-Trp53-
Paxx-/-
Xlf-/-Paxx-/-Trp53-
Mri-/-Paxx-/-
7
11
79
13
9
75
8
15
74
16
3
76
6
8
84
29
2
65
12
7
80
CD43
IgM
B
****p<0.0001
****p<0.0001
IgM+ B cells, %
20
15
10
5
0
WT
Xlf-/-
Mri-/-
Xlf-/-Mri-/-Trp53-
Paxx-/-
Xlf-/-Paxx-/-Trp53-
C
****p<0.0001
****p<0.0001
B220+CD43+IgM-
pro-B cells, %
30
20
10
0
WT
Xlf-/-
Mri-/-
Xlf-/-Mri-/-Trp53-
Paxx-/-
Xlf-/-Paxx-/-Trp53-

Figure 4

A

	Offsprings, P30	Expected, 1:2:1
Paxx$^{-/-}$*Mri*$^{+/+}$	2	3.25
Paxx$^{-/-}$*Mri*$^{+/-}$	4	6.50
Paxx$^{-/-}$*Mri*$^{-/-}$	7	3.25
Total	13	13.00

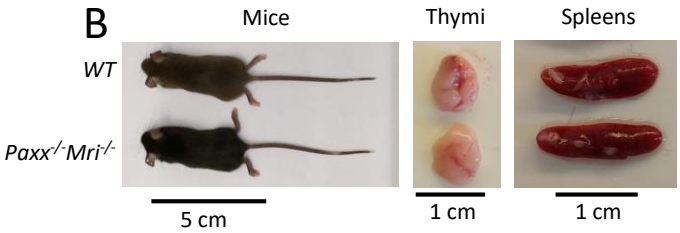

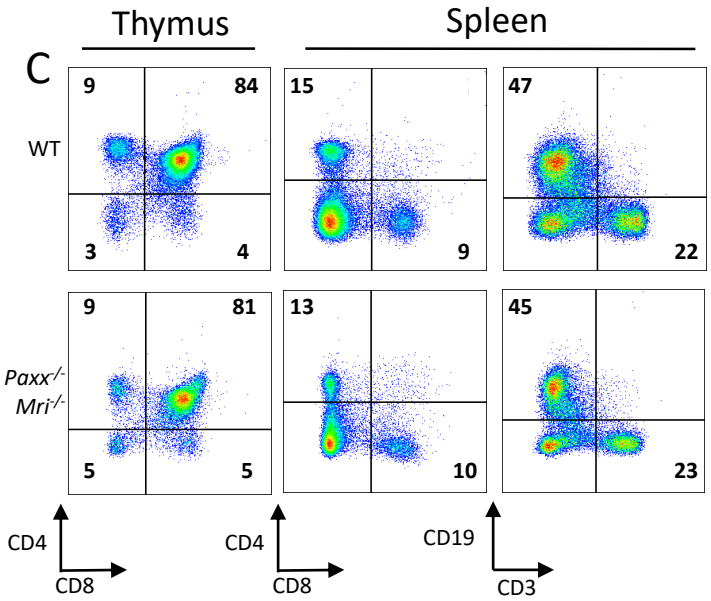

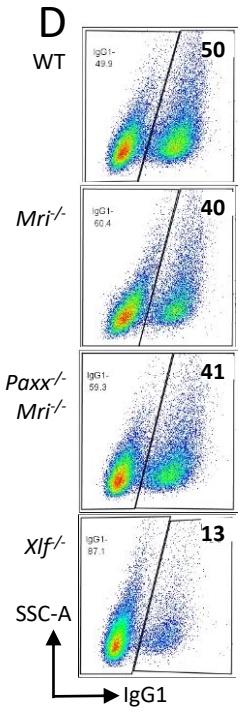

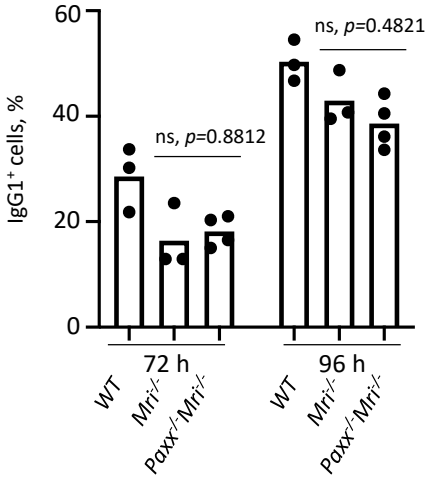

Figure 5

A

	Offsprings, P30	Expected, 1:2:1	*Expected, 1:2:0
Mri$^{-/-}$*Dna-pkcs*$^{+/+}$	12	6	8
Mri$^{-/-}$*Dna-pkcs*$^{+/-}$	12	12	16
Mri$^{-/-}$*Dna-pkcs*$^{-/-}$	**0**	6	0

B

	Offsprings, E14.5	Expected, 1:2:1	*Expected, 1:2:0
Mri$^{-/-}$*Dna-pkcs*$^{+/+}$	1	2.5	3.3
Mri$^{-/-}$*Dna-pkcs*$^{+/-}$	7	5.0	6.7
Mri$^{-/-}$*Dna-pkcs*$^{-/-}$	**2**	2.5	0.0

C

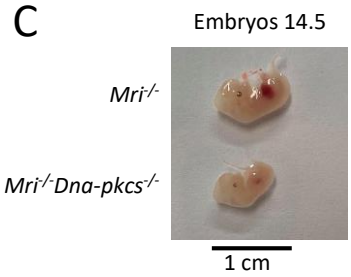

D

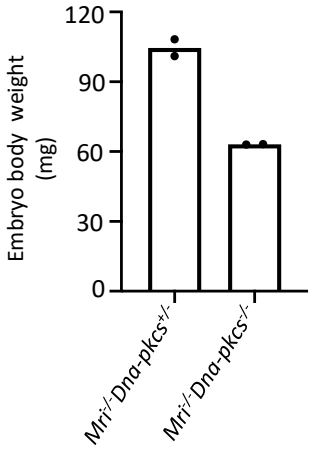

Figure 6

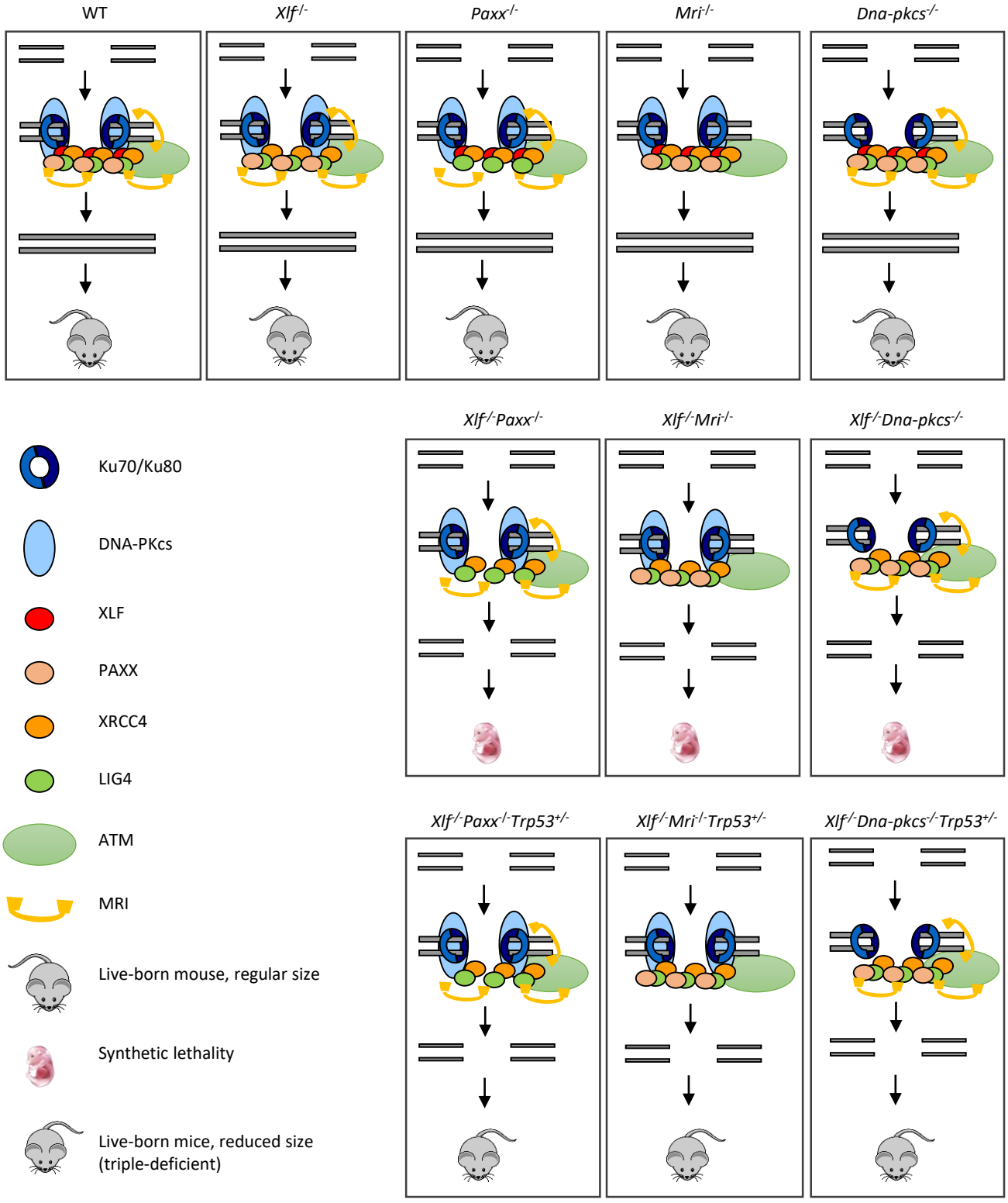
WT
Xlf-/-
Paxx-/-
Mri-/-
Dna-pkcs-/-
Xlf-/-Paxx-/-
Xlf-/-Mri-/-
Xlf-/-Dna-pkcs-/-
Xlf-/-Paxx-/-Trp53+/-
Xlf-/-Mri-/-Trp53+/-
Xlf-/-Dna-pkcs-/-Trp53+/-
Ku70/Ku80
DNA-PKcs
XLF
PAXX
XRCC4
LIG4
ATM
MRI
Live-born mouse, regular size
Synthetic lethality
Live-born mice, reduced size
(triple-deficient)